Physical Mechanism of the Two-Dimensional Enstrophy Cascade

Shiyi Chen,[1,3] Robert E. Ecke,[2] Gregory L. Eyink,[1,4] Xin Wang,[1] and Zuoli Xiao[1]

[1]*Department of Mechanical Engineering, The Johns Hopkins University, Baltimore, Maryland 21218, USA*
[2]*Materials Science & Technology Division, Los Alamos National Laboratory, Los Alamos, New Mexico 87545, USA*
[3]*CCSE and LTCS, Peking University, Peking, China*
[4]*Mathematical Sciences, The Johns Hopkins University, Baltimore, Maryland 21218, USA*

(Received 16 May 2003; published 19 November 2003)

In two-dimensional turbulence, irreversible forward transfer of enstrophy requires anticorrelation of the turbulent vorticity transport vector and the inertial-range vorticity gradient. We investigate the basic mechanism by numerical simulation of the forced Navier-Stokes equation. In particular, we obtain the probability distributions of the local enstrophy flux and of the alignment angle between vorticity gradient and transport vector. These are surprisingly symmetric and cannot be explained by a local eddy-viscosity approximation. The vorticity transport tends to be directed along streamlines of the flow and only weakly aligned down the fluctuating vorticity gradient. All these features are well explained by a local nonlinear model. The physical origin of the cascade lies in steepening of inertial-range vorticity gradients due to compression of vorticity level sets by the large-scale strain field.

DOI: 10.1103/PhysRevLett.91.214501 PACS numbers: 47.27.Ak, 47.27.Gs

Two-dimensional (2D) turbulence has been a fascinating topic for over 30 years, since the seminal papers of Kraichnan [1], Batchelor [2], and Leith [3]. The cascade of enstrophy (mean-square vorticity) to small scales that they proposed is the 2D analog of the energy cascade in three-dimensional (3D) turbulence. One of the reasons for the sustained interest in 2D turbulence is its importance for the interpretation and analysis of atmospheric and oceanic dynamics. Laboratory experiments [4,5] on nearly 2D systems and theoretical advances [6–9] have sparked renewed excitement and interest in the enstrophy cascade. Recent research on 3D turbulence has identified *inertial-range alignments* between characteristic large- and small-scale quantities [10–12], e.g., large-scale strain and small-scale stress, as the key geometrical and statistical property behind the forward energy cascade. One of the crucial goals of turbulence theory is to understand how such alignments are produced by essentially inviscid dynamics at high Reynolds number. Here we explain the origin of the corresponding alignments in 2D, which lead to the forward enstrophy cascade.

We have simulated the equation

$$\partial_t \omega + \mathbf{v}\cdot\boldsymbol{\nabla}\omega + \nu_i(-\Delta)^{-p_i}\omega + \nu_u(-\Delta)^{p_u}\omega = F \quad (1)$$

in a square domain with side $L = 2\pi$ and periodic boundary conditions. Here $\mathbf{v}$ is the velocity and $\omega = \boldsymbol{\nabla}\times\mathbf{v}$ is the vorticity, F (with Fourier components $\hat{F}_{\mathbf{k}} = \eta_{\mathbf{k}}/\hat{\omega}_{-\mathbf{k}}$) is a stirring force applied to wave numbers $|\mathbf{k}| = 4 \rightarrow 7$ to give a constant enstrophy input rate $\eta = \sum_{\mathbf{k}}\eta_{\mathbf{k}}$. We add hyperviscosity with $p_u = 8$ ($\nu_u = 1.4\times 10^{-45}$) at high wave numbers to extend the inertial range and hypoviscosity with $p_i = 2$ ($\nu_i = 16.0$) at small wave numbers to destroy box-size vortices. The equation is solved using a fully dealiased, parallel pseudospectral code with second-order Adam-Bashforth time stepping. The resolution is 2048^2. A statistically stationary state is achieved after 214 large-eddy turnover times. We have also used Laplacian viscosity ($p_u = 1$) to verify that our main results are insensitive to the use of hyperviscosity in Eq. (2).

In Fig. 1, we plot the spectral enstrophy flux $Z(k) = \sum_{|\mathbf{k}|<k}\langle \mathrm{Re}[\hat{\boldsymbol{\omega}}(\mathbf{k})^*(\mathbf{v}\cdot\hat{\boldsymbol{\nabla}}\omega)(\mathbf{k})]\rangle$, showing about a decade and a half of inertial range $20 < k < 500$, where this flux is constant. The inset of Fig. 1 shows the energy spectrum of this final steady state. The power-law scaling in the inertial range is slightly steeper than the -3 law predicted in [1,2] but is consistent with the later logarithmic correction [13]. The figure demonstrates unambiguously the forward flux of enstrophy to smaller scales. It does not, however, describe how the underlying transfer processes are spatially distributed, nor does it suggest how efficient the transfer mechanism is at moving enstrophy to smaller scales. To address these questions, we consider a local flux that quantifies the transfer of enstrophy into small scales at a fixed point in real space.

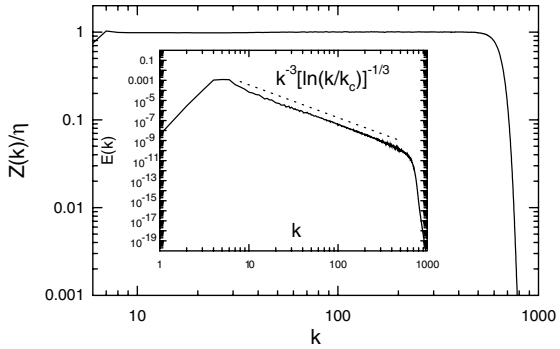

FIG. 1. Enstrophy flux $Z(k)$ normalized by enstrophy dissipation η vs k. The inset is the energy spectrum.

The importance of such a quantity for studying the 3D energy cascade was first emphasized by Kraichnan [14], who defined the local flux by a banded Fourier series. Instead, we distinguish the large- and small-scale modes using a smooth filter as in the large-eddy simulation (LES) modeling scheme [15,16]. We apply the filter to the vorticity form of the 2D Euler equation $\partial_t \boldsymbol{\omega} + (\mathbf{v}\cdot\boldsymbol{\nabla})\boldsymbol{\omega} = 0$. That is, we consider the "large-scale vorticity" defined by the convolution $\overline{\omega}_\ell \equiv G_\ell * \omega$ and the large-scale velocity defined by $\overline{\mathbf{v}}_\ell \equiv G_\ell * \mathbf{v}$, where G_ℓ is taken to be the Gaussian filter. The equation obtained by low-pass filtering is

$$\partial_t \overline{\omega}_\ell(\mathbf{r}, t) + \boldsymbol{\nabla}\cdot[\overline{\mathbf{v}}_\ell(\mathbf{r}, t)\overline{\omega}_\ell(\mathbf{r}, t) + \boldsymbol{\sigma}_\ell(\mathbf{r}, t)] = 0, \qquad (2)$$

where $\boldsymbol{\sigma}_\ell \equiv \overline{(\mathbf{v}\omega)}_\ell - \overline{\mathbf{v}}_\ell\overline{\omega}_\ell$ is the space transport of vorticity due to the eliminated small-scale turbulence. From the previous equation, a balance is derived for the local density $h_\ell(\mathbf{r}, t) = \frac{1}{2}\overline{\omega}_\ell^2(\mathbf{r}, t)$ of the large-scale enstrophy, $\partial_t h_\ell(\mathbf{r}, t) + \boldsymbol{\nabla}\cdot\mathbf{K}_\ell(\mathbf{r}, t) = -Z_\ell(\mathbf{r}, t)$ in which the current $\mathbf{K}_\ell(\mathbf{r}, t) \equiv h_\ell(\mathbf{r}, t)\overline{\mathbf{v}}_\ell(\mathbf{r}, t) + \overline{\omega}_\ell(\mathbf{r}, t)\boldsymbol{\sigma}_\ell(\mathbf{r}, t)$ represents the space transport of large-scale enstrophy, and

$$Z_\ell(\mathbf{r}, t) \equiv -\boldsymbol{\nabla}\overline{\omega}_\ell(\mathbf{r}, t)\cdot\boldsymbol{\sigma}_\ell(\mathbf{r}, t) \qquad (3)$$

is the *enstrophy flux* out of large scales into small-scale modes. This quantity is odd under time reversal—an irreversible forward cascade of enstrophy occurs precisely when it develops a positive mean value. From Eq. (3), we see that in order for Z_ℓ to have a net positive value the turbulent vorticity transport $\boldsymbol{\sigma}_\ell$ should tend to be "down gradient," that is, antiparallel to the large-scale vorticity gradient $\boldsymbol{\nabla}\overline{\omega}_\ell$. The required statistical anticorrelation of $\boldsymbol{\sigma}_\ell$ and $\boldsymbol{\nabla}\overline{\omega}_\ell$ is an *alignment property* characteristic of the 2D enstrophy cascade. It is analogous to the much-studied alignment of the stress tensor $\boldsymbol{\tau}_\ell$ due to small scales and the large-scale strain $\overline{\mathbf{S}}_\ell$, which underlies the energy cascade to high wave numbers in 3D [10–12]. Applying the definitions above to our numerical data computed from (1), we obtain the probability density function (PDF) of the enstrophy flux in the steady-state cascade, $P(Z_\ell)$, shown in Fig. 2(a) for several filtering lengths ℓ in the forward cascade range.

These PDF's have growing tails going to smaller scales, indicating increasing intermittency of the flux. However, the most striking feature of the PDF's are their near symmetry, especially in the far tails. Despite its positive mean (equal to the plateau value in Fig. 1), the skewness of the PDF is quite small, only 1.5. In contrast, the PDF of energy flux in 3D has a skewness of 11 in the inertial range [17]. The forward cascade is made more apparent in Fig. 3(a), where we plot the PDF of the angle of alignment θ between the vectors $\boldsymbol{\sigma}_\ell$ and $\boldsymbol{\nabla}\overline{\omega}_\ell$ for a filtering length $\ell = \pi/130$ in the inertial range (the results are similar throughout that range). There is a greater probability that $\theta > \pi/2$, which occurs about 62% of the time. Since $Z_\ell = |\boldsymbol{\sigma}_\ell|\cdot|\boldsymbol{\nabla}\overline{\omega}_\ell|\cos(\pi - \theta)$,

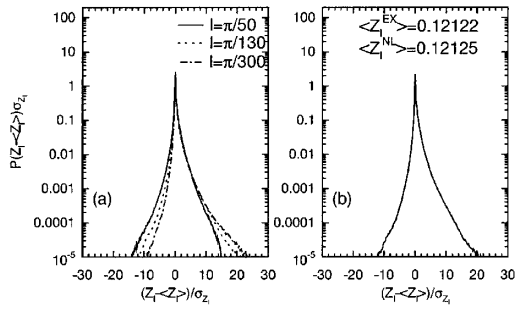

FIG. 2. (a) PDF of $(Z_\ell - \langle Z_\ell\rangle)/\sigma_Z$ with $Z_\ell(\mathbf{r}, t)$ enstrophy flux and $\sigma_Z^2 = \langle(Z_\ell - \langle Z_\ell\rangle)^2\rangle$, at different filter lengths ℓ. (b) PDF's of the true flux (solid line) and the "nonlinear model" (dashed line) at $\ell = \pi/130$. The two lines are indistinguishable.

this is the same as the probability that enstrophy flux is positive. The amplitudes of the flux when positive also tend to be somewhat larger than when negative. This can be seen in Fig. 3(b), which plots the conditional average of Z_ℓ given θ, where the plateau to the right is greater than that to the left. This fact, together with the higher probability of $\theta > \pi/2$, demonstrates that net flux is forward. There is, however, a somewhat greater reluctance of enstrophy in 2D to cascade forward than for energy in 3D. About 70% of the realizations in 3D have positive values of energy flux [17]. Also, the angle between the eigenframes of the minus stress tensor and the filtered strain in 3D is about 32° [12]. It is remarkable that in 2D the most probable value of $\pi - \theta$, the angle between $-\boldsymbol{\sigma}_\ell$ and $\boldsymbol{\nabla}\overline{\omega}_\ell$, is about 77°, much larger than the corresponding angle in 3D. A scalar eddy-viscosity model, as proposed by Leith [18], would give a 0° angle between $-\boldsymbol{\sigma}_\ell$ and

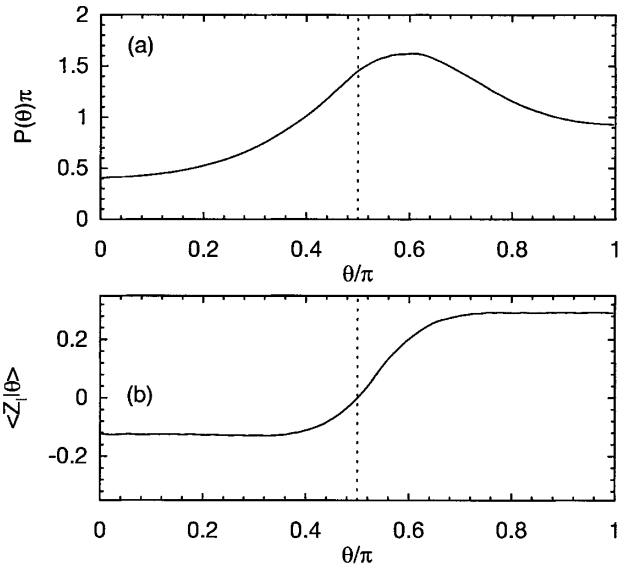

FIG. 3. (a) PDF of the angle θ between $\boldsymbol{\sigma}_\ell$ and $\boldsymbol{\nabla}\overline{\omega}_\ell$ and (b) conditional mean $\langle Z_\ell|\theta\rangle$, for $\ell = \pi/130$.

$\nabla\overline{\omega}_\ell$. Because vorticity gradients tend to be perpendicular to streamlines, Fig. 3(a) shows there is more of a tendency for vorticity transport $\boldsymbol{\sigma}_\ell$ to be parallel to velocity than to be down the local vorticity gradient.

The classical picture of the enstrophy cascade [2,19] is that there is stretching of small-scale vorticity gradients by the strain arising from larger-scale vortices. This suggests that the forward flux should occur mainly in strain-dominated regions of the flow. By the Weiss criterion [20] this corresponds to regions where $\phi_\ell < 0$ (hyperbolic), with $\phi_\ell \equiv \det(\nabla\overline{\mathbf{v}}_\ell) = \frac{1}{2}\overline{\omega}_\ell^2 - \overline{S}_\ell^2$. Regions with $\phi_\ell > 0$ (elliptic) are vorticity dominated. In Fig. 4(a) is plotted the instantaneous $\phi_\ell(\mathbf{r}, t)$ from one snapshot of the simulation, with strain regions in red and vorticity regions in green. In Fig. 4(b) is plotted the instantaneous enstrophy flux in the same domain. The plots show that flux is either forward or backward with almost equal likelihood in vorticity regions, but flux tends to be predominately forward in the strain regions. This is verified quantitatively in Fig. 5(a) which shows the conditional PDF's of the enstrophy flux in both the strain and vorticity regions. The PDF in the strain region is clearly skewed to the right, while the PDF in the vorticity region remains nearly symmetric. The difference between the two regions is seen even more clearly in Fig. 5(b), which plots the conditional PDF's of the angle θ between $\boldsymbol{\sigma}_\ell$ and $\nabla\overline{\omega}_\ell$. The PDF in the strain region is clearly shifted to values of $\theta > \pi/2,$, whereas the PDF in the vorticity region is more nearly symmetric. These results demonstrate that forward enstrophy cascade indeed occurs predominately in strain regions.

The physics of the cascade is further illuminated by a simple approximation for $\boldsymbol{\sigma}_\ell$ [9]. To derive this expression we introduce a new length scale $\tilde{\ell} \le \ell$ and low-pass filter $\tilde{\mathbf{v}}$ of $\mathbf{v}$ with scales less than $\tilde{\ell}$ removed. Then, for $\tilde{\ell} < \ell$ it should be true that $\boldsymbol{\sigma}_\ell \approx \overline{\tilde{\mathbf{v}}\,\tilde{\boldsymbol{\omega}}} - \tilde{\mathbf{v}}\,\tilde{\boldsymbol{\omega}}$. The scales less than $\tilde{\ell}$ are believed to make only a disorganized, uncoordinated contribution to the vorticity transport $\boldsymbol{\sigma}_\ell$ [13]. Although vorticity increments at smaller scales decrease only very slowly, in mean square as $\log(\tilde{\ell})$, contributions of those scales are subject to large cancellations, producing an extra small factor $\tilde{\ell}$. The resulting approximation is a 2D analog of the similarity model [15], a computational LES model in 3D. We emphasize, however, that our approximation does not rely on any phenomenological assumption of self-similarity, but only on the assumption that scales $\tilde{\ell} < \ell$ contribute negligibly. We have verified that the approximate formula for the transport vector is almost indistinguishable from the exact one for all $\tilde{\ell} < \ell$. For the extreme choice $\tilde{\ell} = \ell$ the fields appearing in the formula for $\boldsymbol{\sigma}_\ell$ are smooth on the filter scale ℓ and their increments over such lengths can be approximated by a local Taylor expansion. The leading-order term is the analog of the 3D nonlinear model [15]:

$$\boldsymbol{\sigma}_\ell^{\mathrm{NL}} = C_2\ell^2\overline{\mathbf{D}}_\ell\cdot\nabla\overline{\boldsymbol{\omega}}_\ell, \tag{4}$$

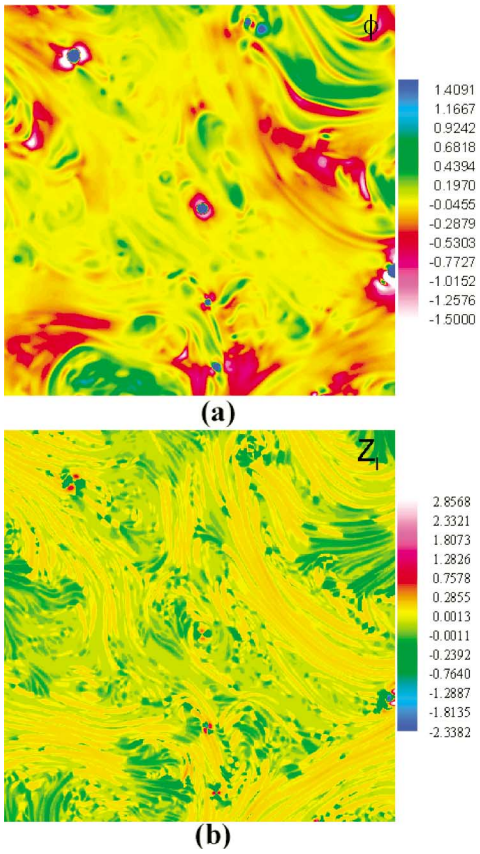

FIG. 4 (color). Instantaneous snapshot of (a) $\phi_\ell(\mathbf{r}, t)$ and (b) $Z_\ell(\mathbf{r}, t)$, for $\ell = \pi/130$ in a 512^2 subdomain. The red regions in (a) are dominated by strain and the green by vorticity.

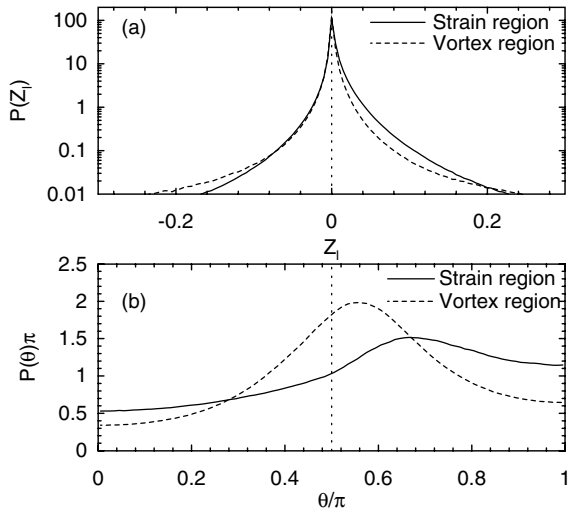

FIG. 5. (a) PDF's of $Z_\ell(\mathbf{r}, t)$ and (b) PDF's of the angle θ between $\boldsymbol{\sigma}_\ell$ and $\nabla\overline{\omega}_\ell$, $\ell = \pi/130$. The solid line indicates strain, and the dashed line indicates the vorticity region. $\langle Z_\ell\rangle_{\mathrm{strain}} = 3.7 \times 10^{-3}$ and $\langle Z_\ell\rangle_{\mathrm{vortex}} = 9.5 \times 10^{-4}$.

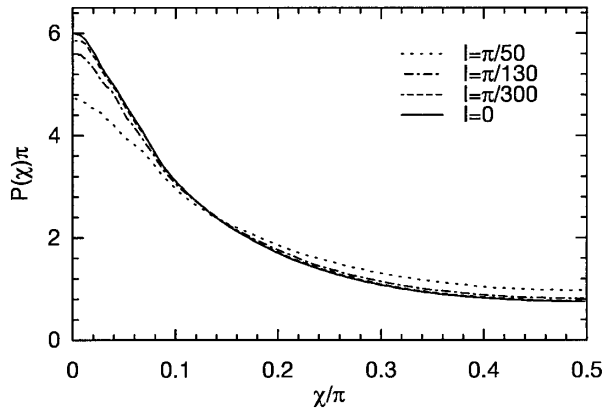

FIG. 6. PDF's of the angle χ between $\nabla\overline{\omega}_\ell$ and $\boldsymbol{l}_\ell^-$, the left eigenvector of $\mathbf{D}_\ell$ for the negative eigenvalue.

where $\overline{D}_{ij} = \partial\overline{v}_i/\partial x_j$ is the large-scale velocity gradient (or deformation) tensor and C_2 is the second moment of the filtering function G. The expression $C_2\ell^2\overline{\mathbf{D}}_\ell$ in (4) is a "tensor eddy viscosity," which scales dimensionally the same as the scalar eddy viscosity proposed by Leith [18]. The arguments of Kraichnan [21] cast doubt on the validity of a scalar eddy viscosity, and, indeed, we have verified that a perfect antiparallel alignment of $\boldsymbol{\sigma}_\ell$ and $\nabla\overline{\omega}_\ell$ is not observed. However, the tensor eddy-viscosity model of the transport vector in (4) is correlated with the exact one at the 99% level. The two vector fields, $\sigma_\ell(\mathbf{r}, t)$ and $\sigma_\ell^{\mathrm{NL}}(\mathbf{r}, t)$, in a plot together (not shown) are almost identical to the eye. The PDF of the nonlinear model approximation to the enstrophy flux, $Z_\ell^{\mathrm{NL}} = -C_2\ell^2(\nabla\overline{\omega}_\ell)^\top\overline{\mathbf{D}}_\ell\cdot\nabla\overline{\omega}_\ell$, shown in Fig. 2(b), is likewise nearly indistinguishable from the exact PDF.

The close agreement of the exact transport vector $\boldsymbol{\sigma}_\ell$ and $\boldsymbol{\sigma}_\ell^{\mathrm{NL}}$ allows us to connect the forward flux more clearly with the physical picture of the enstrophy cascade. This is believed to be due to the stretching and compression of ribbons of vorticity by the large-scale strain field. In fact, the squeezing together of very different vorticity levels amplifies the gradient along the compressive direction. Therefore, one expects that $\nabla\overline{\omega}_\ell$ will tend to align in the strain regions along $\boldsymbol{l}_\ell^-$, the left eigenvector of $\overline{\mathbf{D}}_\ell$ for the negative eigenvalue. In Fig. 6 is plotted the PDF of the angle between $\nabla\overline{\omega}_\ell$ and $\boldsymbol{l}_\ell^-$. There is an increasing tendency for these vectors to align as ℓ decreases through the inertial range. The corresponding alignment for the dissipation-range quantities, with $\ell = 0$, was already observed in [22,23]. In view of the formula for Z_ℓ^{NL} this typical alignment explains the tendency for flux to be positive. If the alignment were perfect, then a scalar eddy-viscosity model would result, with $\boldsymbol{\sigma}_\ell = -C_2\gamma_\ell\ell^2\nabla\overline{\omega}_\ell$, where $\pm\gamma_\ell$ are the eigenvalues of $\overline{\mathbf{D}}_\ell$ (both real in the strain region). As shown in Fig. 6 this alignment is the most likely, but not overwhelmingly so. Thus, the enstrophy flux is often negative as well as positive, but preferentially positive in the strain region.

In conclusion, we have shown that the 2D enstrophy cascade is surprisingly time symmetric. Turbulent vorticity transport tends to be along streamlines, not down gradient as predicted by a scalar eddy viscosity. A tensor viscosity model, the nonlinear model, predicts well the transport vector, making the model attractive for geophysical applications. Our work has clarified the fundamental connection of 2D enstrophy cascade to stretching of inertial-range vorticity gradients.

We thank Q. Chen, R. Kraichnan, C. Meneveau, M. Nelkin, M. Rivera, and B. Daniel for discussions. Simulations were run on the cluster computer supported by NSF Grant No. CTS-0079674 at Johns Hopkins University and in LSSC-II at the State Key Laboratory on Scientific and Engineering Computing in China.

[1] R. H. Kraichnan, Phys. Fluids **10**, 1417 (1967).
[2] G. K. Batchelor, Phys. Fluids **12**, II-233 (1969).
[3] C. E. Leith, Phys. Fluids **11**, 671 (1968).
[4] M. K. Rivera, P. Vorobieff, and R. E. Ecke, Phys. Rev. Lett. **81**, 1417 (1998).
[5] J. Paret, M.-C. Jullien, and P. Tabeling, Phys. Rev. Lett. **83**, 3418 (1999).
[6] K. Ohkitani, Phys. Fluids A **2**, 1529 (1990).
[7] J.-P. Laval, B. Dubrulle, and S. Nazarenko, Phys. Rev. Lett. **83**, 4061 (1999).
[8] P.-H. Chavanis, Phys. Rev. Lett. **84**, 5512 (2000).
[9] G. L. Eyink, Nonlinearity **14**, 787 (2001).
[10] V. Borue and S. A. Orszag, J. Fluid Mech. **366**, 1 (1998).
[11] M. Chertkov, A. Pumir, and B. I. Shraiman, Phys. Fluids **11**, 2394 (1999).
[12] B. Tao, J. Katz, and C. Meneveau, J. Fluid Mech. **457**, 35 (2002).
[13] R. H. Kraichnan, J. Fluid Mech. **47**, 525 (1971).
[14] R. H. Kraichnan, J. Fluid Mech. **62**, 305 (1974).
[15] C. Meneveau and J. Katz, Annu. Rev. Fluid Mech. **32**, 1 (2000).
[16] G. L. Eyink, J. Stat. Phys. **78**, 335 (1995).
[17] Q. Chen, S. Chen, G. Eyink, and D. Holm, Phys. Rev. Lett. (to be published).
[18] C. E. Leith, in *Properties of Matter Under Unusual Conditions* (Interscience, New York, 1969), pp. 267–271.
[19] R. H. Kraichnan, J. Fluid Mech. **67**, 155 (1975).
[20] J. Weiss, Physica (Amsterdam) **48D**, 273 (1987); see also C. Basdevant and T. Philipovitch, Physica (Amsterdam) **73D**, 17 (1994).
[21] R. H. Kraichnan, J. Atmos. Sci. **33**, 1521 (1976).
[22] M. E. Brachet *et al.*, J. Fluid Mech. **194**, 333 (1988).
[23] B. Protas, A. Babiano, and N. K.-R. Kevlahan, Physica D (Amsterdam) **128**, 169 (1999).